Investigation of magneto-structural phase transition in FeRh by reflectivity and transmittance measurements in visible and near-infrared spectral region

2016 New J. Phys. 18 083017

(http://iopscience.iop.org/1367-2630/18/8/083017)

New Journal of Physics
The open access journal at the forefront of physics

Deutsche Physikalische Gesellschaft DPG
IOP Institute of Physics

Published in partnership with: Deutsche Physikalische Gesellschaft and the Institute of Physics

OPEN ACCESS

RECEIVED
12 April 2016

REVISED
30 June 2016

ACCEPTED FOR PUBLICATION
18 July 2016

PUBLISHED
3 August 2016

PAPER

Investigation of magneto-structural phase transition in FeRh by reflectivity and transmittance measurements in visible and near-infrared spectral region

V Saidl[1], M Brajer[1], L Horák[1], H Reichlová[2], K Výborný[2,5], M Veis[1], T Janda[1], F Trojánek[1], M Maryško[2], I Fina[3], X Marti[2,3], T Jungwirth[2,4] and P Němec[1]

[1] Faculty of Mathematics and Physics, Charles University in Prague, CZ–12116 Praha 2, Czech Republic
[2] Institute of Physics, Academy of Sciences of the Czech Republic, v.v.i., CZ–16253 Praha 6, Czech Republic
[3] ICN2-Institut Català de Nanociència i Nanotecnologia, Campus Universitat Autònoma de Barcelona, E–08193 Bellaterra, Spain
[4] School of Physics and Astronomy, University of Nottingham, NG7 2RD Nottingham, UK
[5] Author to whom any correspondence should be addressed.

E-mail: vybornyk@fzu.cz **and** nemec@karlov.mff.cuni.cz

Keywords: antiferromagnet, phase transition, optical permittivity

Abstract

Magneto-structural phase transition in FeRh epitaxial layers was studied optically. It is shown that the transition between the low-temperature antiferromagnetic phase and the high-temperature ferromagnetic phase is accompanied by a rather large change of the optical response in the visible and near-infrared spectral ranges. This change is consistent with *ab initio* calculations of reflectivity and transmittance. Phase transition temperatures in a series of FeRh films with thicknesses ranging from 6 to 100 nm is measured thereby demonstrating the utility of the method to quickly characterise samples. Spatially resolved imaging of their magnetic properties with a micrometer resolution shows that the phase transition occurs at different temperatures in different parts of the sample.

1. Introduction

The near-equiatomic alloy of iron and rhodium undergoes a first-order magneto-structural transition from an antiferromagnetic (AF) to ferromagnetic (FM) phase around 380 K. Even though this discovery is more than seventy years old [1] it still attracts significant attention nowadays. One of the reasons is that this transition occurs close to the room temperature and unlike in certain perovskites [2], FeRh is naturally a metal, which makes it appealing for applications. For example, exchange-coupled FePt/FeRh thin films were used by Thiele *et al* in 2003 [3] to improve the long-time stability of a material used in thermally assisted magnetic recording and to lower the coercive field [4]. More recently, a room-temperature antiferromagnetic memory resistor based on FeRh was reported by Martí *et al* [5] thus demonstrating the feasibility of the antiferromagnetic spintronics concept [6]. Also in 2014, Cherifi *et al* reported [7] the electric-field control of the transition temperature in a FeRh film grown on a ferroelectric substrate $BaTiO_3$. Lee *et al* used the strain-mediated change in relative proportions of the AF and FM phases to construct a memory device based on FeRh/PMN-PT [8]. Moreover, it was shown that the change of the magnetic order can be rather fast—AF to FM transition can be induced by laser pulses on the picosecond time scale [9].

Research on FeRh was originally conducted on bulk samples [1, 10–12] but more recently, due to the envisioned applications [3, 5, 8], it focuses on thin films. The desired AF phase is present only for a rather narrow interval of the Fe-to-Rh composition ratios [12], which are achieved experimentally by a variation of the deposition conditions [13–15] and by a post-preparation heat treatment [16]. Consequently, the growth of high quality FeRh thin films is a rather complex task which requires a lot of optimisation of the preparation procedure and a deposition of large series of samples [13–16]. The magnetic phase transition in the prepared films is usually studied by magnetometry, for example by superconducting quantum interference device (SQUID), where not only the phase transition temperature but also the remaining uncompensated magnetic moment in the low-

temperature AF phase is measured [14, 15]. However, the disadvantage of magnetometry is that the magnetic properties are averaged over the whole sample and that it is necessary to subtract the substrate contribution from the measured data. Also, temperature can usually be increased only up to 400 K in a typical SQUID apparatus and this is often not sufficient to fully convert the AF into the FM phase. Therefore both, the transition temperature and the magnetisation in the FM phase may be measured inaccurately in such experiments. Alternatively, the transition temperatures can be determined from measurements of the resistivity [10] or magneto-optical response [16].

In this article, we show that the AF to FM phase transition can be also studied by the most straightforward optical experiment where the sample transmission and/or reflectivity is measured while the sample temperature is varied. Contrary to previous claims [17], we observe a clear change of optical properties of FeRh thin films upon crossing the AF to FM transition and find it to be most significantly pronounced in the near infrared spectral range. To demonstrate the applicability of this experimental technique for a fast characterisation of FeRh layers, we use it to obtain spatially resolved images which reveal magnetic inhomogeneity of one part of the investigated sample.

Reports about experimentally measured optical properties (permittivity) of FeRh are very limited. Ellipsometric measurements of optical constants in bulk FeRh reported by Sasovskaja and Noskov in 1974 concern the mid-infrared spectral region [11]. A clear hysteretic behaviour of the sample reflectivity was observed as the temperature was swept back and forth between 293 and 423 K. In contrast, no appreciable change of optical constants at the AF to FM transition was reported by Rhee and Lynch in 1995 [17] who applied conventional ellipsometry to FeRh in the spectral region of visible and UV light. The same author points out in [12] the implication of these measurements that the band structure of FeRh is less affected by the AF to FM phase transition than *ab initio* calculations would indicate. We note that this statement contradicts later non-optical experimental [18, 19] and theoretical [18, 20] publications. In particular, clear differences between the AF and FM states were observed in recent hard x-ray photoemission spectroscopy experiments [18]. These differences occur across the entire spectrum and they are well reproduced by density-functional calculations.

2. Samples and experimental setup

Four FeRh films with thicknesses of 6, 18, 36 and 100 nm were grown on double-side polished MgO (001) substrates by dc sputtering. Firstly, substrates were heated up to 550 K in a base pressure of 10^{-8} Torr. Afterwards, Ar gas was introduced (3 mTorr) and the films were grown using power of 50 W at a rate of 1 nm per 1 min using a stoichiometric FeRh target. Finally, the films were protected by a tantalum cap. After deposition, the films were heated up to 770 K at a rate of 10 K min^{-1} in vacuum, annealed for 1 h and subsequently cooled to room temperature at the same rate. The high magnetic and structural quality of all the investigated samples was confirmed by SQUID, x-ray reflectivity (XRR) and x-ray diffraction (XRD) measurements.

As detailed in appendix D, it follows from XRD that all investigated FeRh films are monocrystalline with the lattice azimuthally rotated by 45° with respect to the MgO substrate lattice. The XRD reciprocal space mapping in figure 11 shows that the lattice of the thickest film is fully relaxed, i.e., it keeps the cubic symmetry. The lattice of other investigated films is tetragonally distorted to match the lateral periodicity of the MgO substrate. The thickness of each film was determined using XRR. Moreover, using this surface-sensitive method we were able to determine the thickness of the FeRh film and of the capping layer. Magnetic properties of the samples (see appendix A) were measured using quantum design SQUID with a 4 cm long reciprocating sample option. Data measured above 400 K were obtained using a high-temperature insert.

Standard reflectivity ($R = I_R/I_0$) and transmittance ($T = I_T/I_0$) spectra were computed from the spectral dependences of the reflected (I_R), transmitted (I_T) and incident (I_0) light intensity measured by grating spectrographs equipped with CCD (USB2000+, Ocean Optics). Typical transmittance ranged from 45% in the thinnest to 0.2% in the thickest sample and reflectances were more than 30% for all samples. A standard tungsten lamp was used as a light source. The reflectivity spectra were further corrected for the chromatic aberrations in the experimental setup by comparing the obtained reflectivity spectrum to a reference GaAs sample, whose theoretical spectrum was computed from the tabulated optical constants of GaAs [21]. The transmittance spectra of the FeRh films were corrected for the transmittance and the reflectivity of the MgO substrate. No external magnetic field was applied during the optical measurements. The samples were placed in a vacuum on a cold finger of a closed-cycle cryostat (Advanced Research Systems) where the temperature can be changed from 8 to 800 K. To measure the spatially resolved reflectivity images, we used a home-made microscope equipped with an objective lens (MitutoyoM Plan Apo, magnification 20×, numerical aperture 0.42) and CCD camera (Allied Vision Tech, model Prosilica GX 1050) which provided images of the sample surface with a spatial resolution of 1 μm. In this experiment we used continuous-wave Ti:sapphire laser as a light

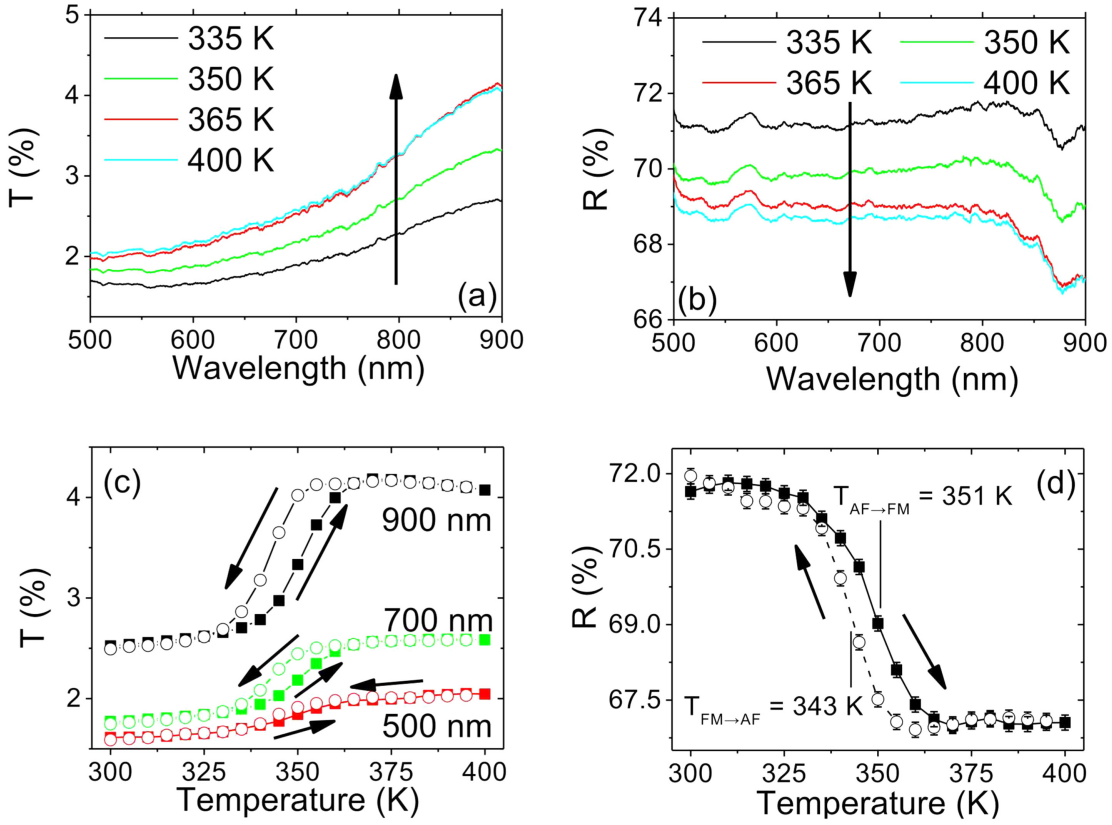

Figure 1. Temperature dependence of the optical response in the 36 nm thick FeRh film. (a) Transmittance (T) and (b) reflectivity (R) spectra measured for increasing sample temperature. (c) Temperature dependence of transmittance at 500, 700 and 900 nm. (d) Temperature dependence of reflectivity at 900 nm with depicted transition temperatures $T_{AF\rightarrow FM}$ and $T_{FM\rightarrow AF}$. Arrows indicate the temperature change direction.

source. To suppress the laser light coherence we used a laser speckle reducer (Optotune, LSR-3005-24D-VIS) in the illumination beam.

3. Reflectivity and transmittance: measurement and *ab initio* modelling

Transmittance and reflectivity spectra that were measured simultaneously during the heating and the successive cooling of the 36 nm thick FeRh film are shown in figure 1. We observed that the temperature-induced AF-to-FM phase transition leads to an increase of the sample transmittance (figure 1(a)) and to a decrease of the sample reflectivity (figure 1(b)). For example, at 800 nm, the measured transmittance increase of 1% and the reflectivity decrease of 3% indicate the film absorption increase of 2%, a change that can be easily detected. We observed similar behaviour with other samples as shown in appendix C. Below, we argue that the observed change originates indeed from the FeRh layer and this invalidates the claims of Rhee and Lynch [17] of no appreciable change in the dielectric function as the AF-to-FM phase transition in FeRh is traversed.

To complete our claim and to understand the origin of this experimental finding, we performed an *ab initio* based model calculation of the spectral form of T and R in the FM and AF phase. Our model assumes a multilayer structure (1.5 nm thick Ta capping layer, 36 nm of FeRh and an infinite MgO substrate) as the input to the 4×4 transfer matrix approach for anisotropic multilayers [22]. The real and imaginary parts of permittivity of the individual materials were calculated using the full-potential linearised-augmented-plane-wave method (WIEN2k package [23]) for FeRh and taken from the literature in the case of Ta [24] and MgO [25]. All calculations were performed assuming zero temperature and the high (low) temperature phase investigated in our experiments was modelled by assuming the FM (AF) magnetic structure and appropriate lattice constants as described in appendix B. In there, we also discuss the individual effect of the intra- and inter-band contributions to permitivity spectra.

Real and imaginary parts of the complex permittivity $\varepsilon' + i\varepsilon''$ are shown in figures 2(a) and (b), respectively. Obtained transmittance and reflectivity spectra, which are shown in figures 2(c) and (d), agree qualitatively with the measurements. In particular, they show an increase (decrease) of transmittance (reflectivity) by a few percent

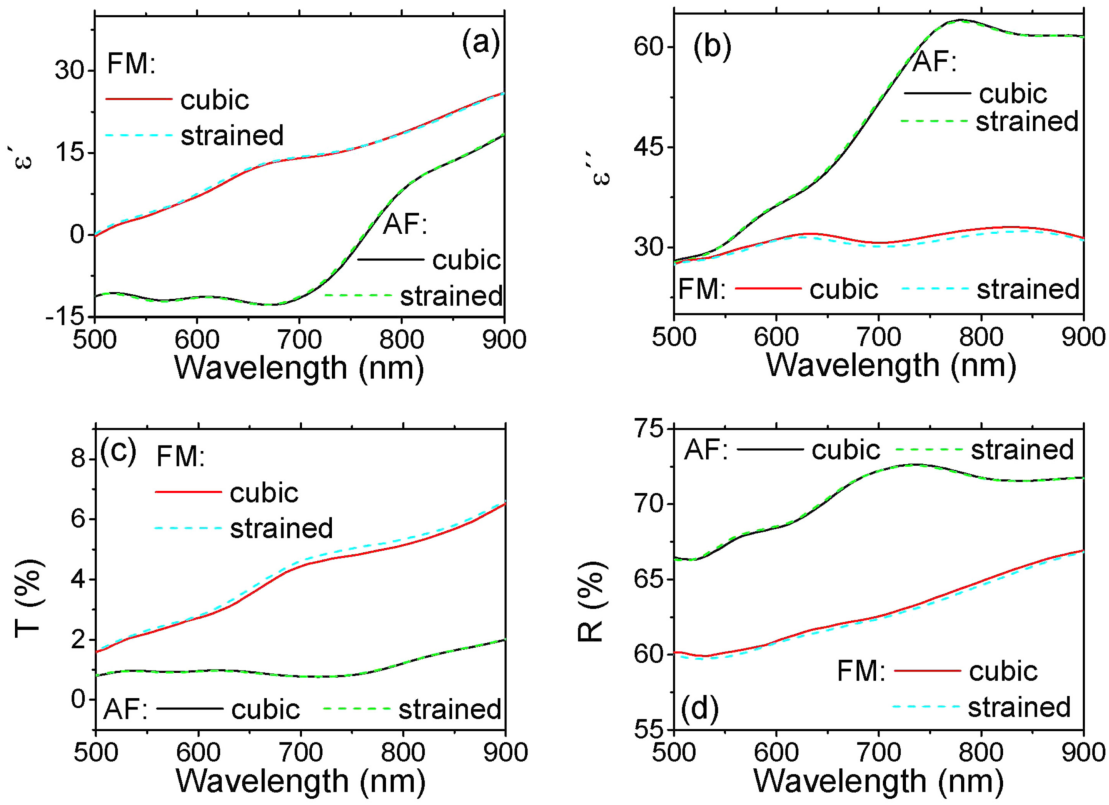

Figure 2. Calculated spectral dependence of optical parameters of the antiferromagnetic (low-temperature) and ferromagnetic (high-temperature) phase of FeRh for bulk cubic crystal structure and for tetragonal structure in strained thin film. (a) Real (ε') and (b) imaginary (ε'') part of permittivity of FeRh. Multilayer Ta/FeRh/MgO spectra of transmittance (c) and reflectivity (d).

upon the transition from the AF to FM phase. Quantitative differences between the model and the experiment, seen in particular in the reflection, are likely a consequence of the samples being exposed to air. The XRR measurements indicate that the Ta capping layer has been oxidised to certain extent, hence its actual optical properties may be different from those of pure tantalum.

In order to explore further the origin of the measured change in optical properties, we compared theoretically the case where both magnetic phases were cubic (bulk-like) to the case of thin film where they were tetragonal due to the MgO substrate-induced strains [26] (MgO has a smaller lattice constant than bulk FeRh). The strains are smaller in the AF phase than in the FM phase, which has a larger lattice constant in the bulk [26] and the specific lattice constants used in our calculations are given in appendix B. We found that the substrate-induced strains do change the permittivity (and consequently the layer transmittance and reflectivity) but the changes are minute. Our conclusion is therefore that the experimentally observed changes of optical properties are indeed due to the AF-to-FM transition rather than due to the thin film nature of the studied samples and they should be equally present also in bulk FeRh samples.

4. Spatially resolved measurements

In contrast to transport and SQUID magnetometry measurements, optical techniques afford the opportunity to obtain spatially resolved information on the phase transition in a FeRh sample. Below, we compare the global and the local look at the 36 nm thick FeRh film in transmittance and reflectivity.

The measured hysteretic optical properties can be used to evaluate the characteristic temperatures describing the AF-to-FM ($T_{AF\rightarrow FM}$) and FM-to-AF ($T_{FM\rightarrow AF}$) transitions [27] which we define as the mean temperature between the onset and end of the optical properties change [28, 29]. These observations by optical means are well correlated with magnetometry results (see appendix A), hence reflectivity measurements (e.g. as a function of temperature) can be used as an alternative to the determination of $M(T)$ using SQUID. From data shown in figures 1(c) and (d) we obtained $T_{AF\rightarrow FM} = 351 \pm 2$ K and $T_{FM\rightarrow AF} = 343 \pm 2$ K, respectively, regardless of the wavelength at which the transition was observed. For practical purposes of detecting the transition, red and infrared spectral regions are the most suitable in the reflection geometry where the relative change of signal is around 5%, see figure 1(d). In the transmission geometry, the relative change of the signal is larger than that for

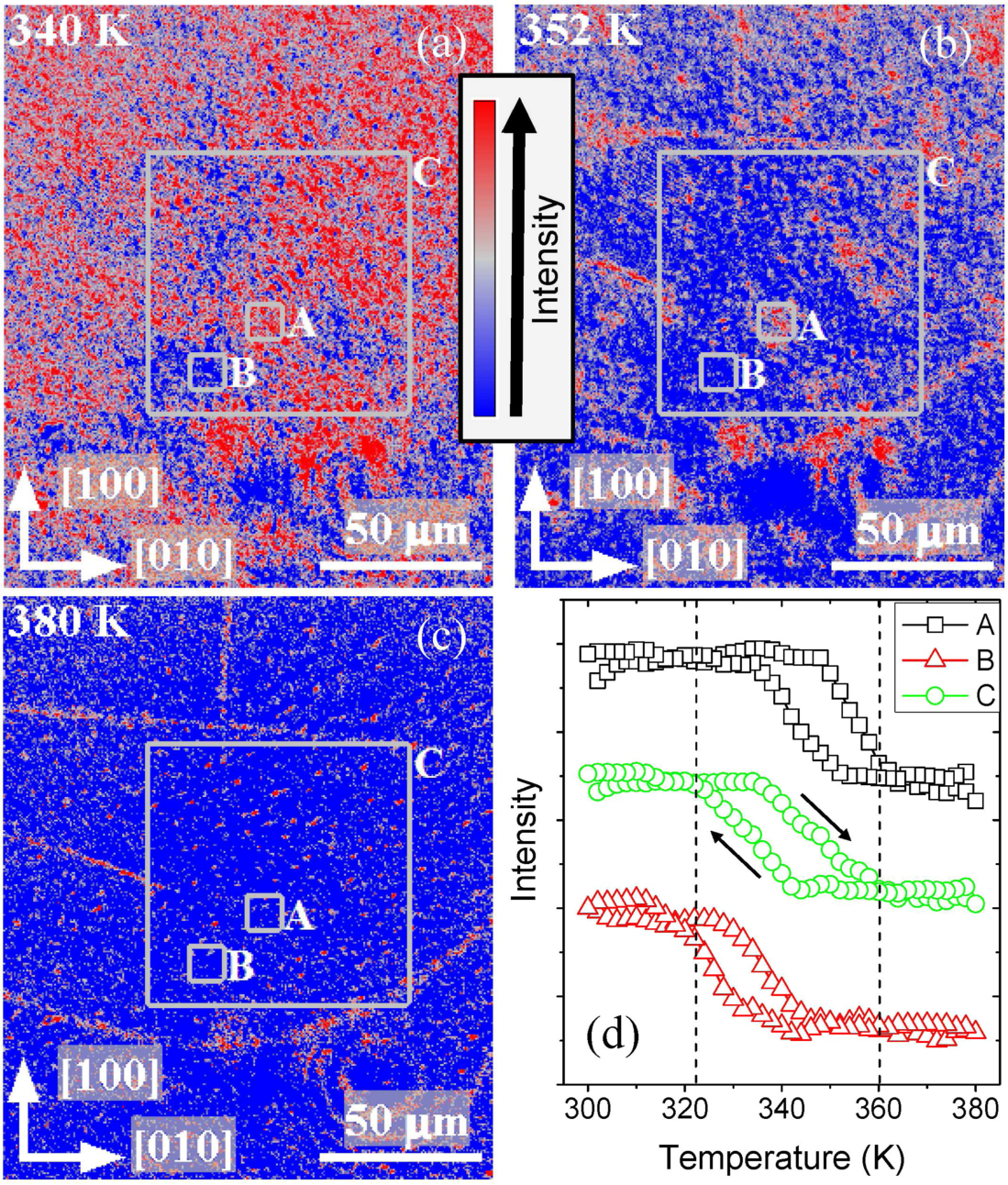

Figure 3. Images of spatially resolved reflectivity change at 950 nm obtained during heating of the 36 nm FeRh film at (a) 340 K, (b) 352 K, (c) 380 K. From the as-measured images the reflectivity map obtained at 300 K was subtracted and the resulting image was colour encoded: dark red colourno change of reflectivity (i.e., it corresponds to the antiferromagnetic phase with larger reflectivity), dark blue colourmaximally reduced reflectivity (i.e., it corresponds to the ferromagnetic phase with smaller reflectivity). (d) Reflected intensity of light spatially averaged within the sample areas A, B, and C depicted in the images; the curves were vertically shifted for clarity.

all wavelengths in the studied spectral range (500–900 nm), see figure 1(c), hence transmission measurements may be considered more advantageous. Figure 3 of [11] suggests that even mid-infrared range could be used. We note that these observations have rather strong implications for a practical realisation of optical experimental setups where large quantities of prepared samples can be routinely tested during the FeRh films optimisation. If relatively thin (up to ≈50 nm) FeRh films are prepared on double-side polished transparent substrates, then basically any available light source can be used to detect the magnetic phase transition in the transmission geometry. For thicker films, the experiment has to be performed in the reflection geometry and the GaAs-based lasers working in the near infrared spectral region, which are fully compatible with silicon detectors, are probably the best choice from the point-of-view of the stability and acquisition price of the optical characterisation setup.

Spatially resolved reflectivity change of one part of the 36 nm FeRh film obtained while the sample was heated up is shown in figures 3(a)–(c). The reflectivity map obtained at 300 K was subtracted from all the as-measured images and the resulting image (i.e., the spatially resolved reflectivity change) was colour encoded: dark red corresponds to the original (higher) reflectivity and dark blue corresponds to the maximally reduced reflectivity in the FM phase. Apparently, the magnetic phase transition occurs at different temperatures in different regions of the sample. This is visible even more clearly in figure 3(d), where the reflected intensity of light is shown spatially averaged within the sample areas A and B which have dimensions of $10 \times 10\ \mu m^2$. We obtained $T_{AF\rightarrow FM} = 355 \pm 2$ K and $T_{FM\rightarrow AF} = 342 \pm 2$ K for A and $T_{AF\rightarrow FM} = 336 \pm 2$ K and $T_{FM\rightarrow AF} = 326 \pm 2$ K for B. If the signal is averaged over a considerably larger area C, which is the case for experiments without the spatial resolution, the deduced hysteresis loops are less sharp and the obtained characteristic temperatures are $T_{AF\rightarrow FM} = 347 \pm 2$ K and $T_{FM\rightarrow AF} = 334 \pm 2$ K. In addition to the existence of regions A and B, where the magnetic phase transition is shifted in temperature by ≈19 K, there are also sample parts that do not change their reflectivity at all (during the temperature increase up to 400 K). These regions appear in figure 3(c) as red spots (typically with a diameter of ≈2 μm) or lines (with a width of ≈3 μm and a length exceeding ≈100 μm). They originate from sample parts where the material remains in the ferromagnetic state even up to 400 K and/or from areas where the FeRh film is completely absent. Note that for this particular experiment we deliberately selected a part of the sample which was partially mechanically damaged in order to better demonstrate the potential of spatially resolved optical techniques.

5. Conclusions

We have shown experimentally that the first-order magneto-structural transition in FeRh is clearly pronounced also in the optical response of this material, especially in the near infrared spectral range. Our *ab initio* calculations indicate that the modification of optical constants have a similar magnitude both in thin films and in bulk material. Spatially resolved measurement of the sample magnetic homogeneity, which is a very important issue for the preparation of envisioned devices[6], showed that the antiferromagnet-to-ferromagnet transition can take place at different temperatures in different regions of the FeRh film. In our sample, variations of the transition temperature were around 20 K.

Acknowledgments

The authors are indebted to R Ramesh and S Salahuddin for preparation of samples. We gratefully acknowledge the assistance of Jakub Železný and Martin Ondráček with *ab initio* calculations. This work was supported by the Grant Agency of the Czech Republic under Grant 14-37427G, by ERC Advanced Grant 268066 (0MSPIN), and by Grant Agency of Charles University in Prague Grants 1910214 and SVV-2015-260216.

Appendix A

The temperature dependence of magnetisation measured by SQUID in the studied films is shown in figure 4. The high magnetic quality of all the investigated samples is confirmed by a negligible moment in the AF phase and the expected [3, 13] magnitude of the magnetic moment in the FM phase. The magnetisation is smaller in the 6 nm film (see figure 4), and we attribute this fact to the presence of a magnetically dead layer [30]. Note that the transition temperatures obtained by SQUID are shifted to lower temperatures due to the applied magnetic field [27]. Since measured profiles of $M(T)$ in figure 4 are very similar to the reflectivity and transmittance shown in figures 1(c), (d) and 8, we conclude that opticals measurements can be used as an alternative to SQUID.

Appendix B

Input parameters of the *ab initio* calculation

Bulk iron rhodium alloy has the cubic structure of caesium chloride with lattice constant $a_{lc}^{FeRh} = 0.2986$ nm at room temperature [31]. Type-II ordering in the AF phase is shown in figure 5. Upon heating, the alloy becomes ferromagnetically ordered and while the lattice constant expands as measured by Ibarra and Algarabel [32], the crystal structure remains unchanged. In accord with these measurements, our calculations of optical properties for the cubic AF (FM) case shown in figures 2(a) and (b) assume the lattice constant 0.2986 nm (0.2998 nm).

[6] Some of the proposed device concepts are summarised in the first paragraph of the introduction under [3, 5–8].

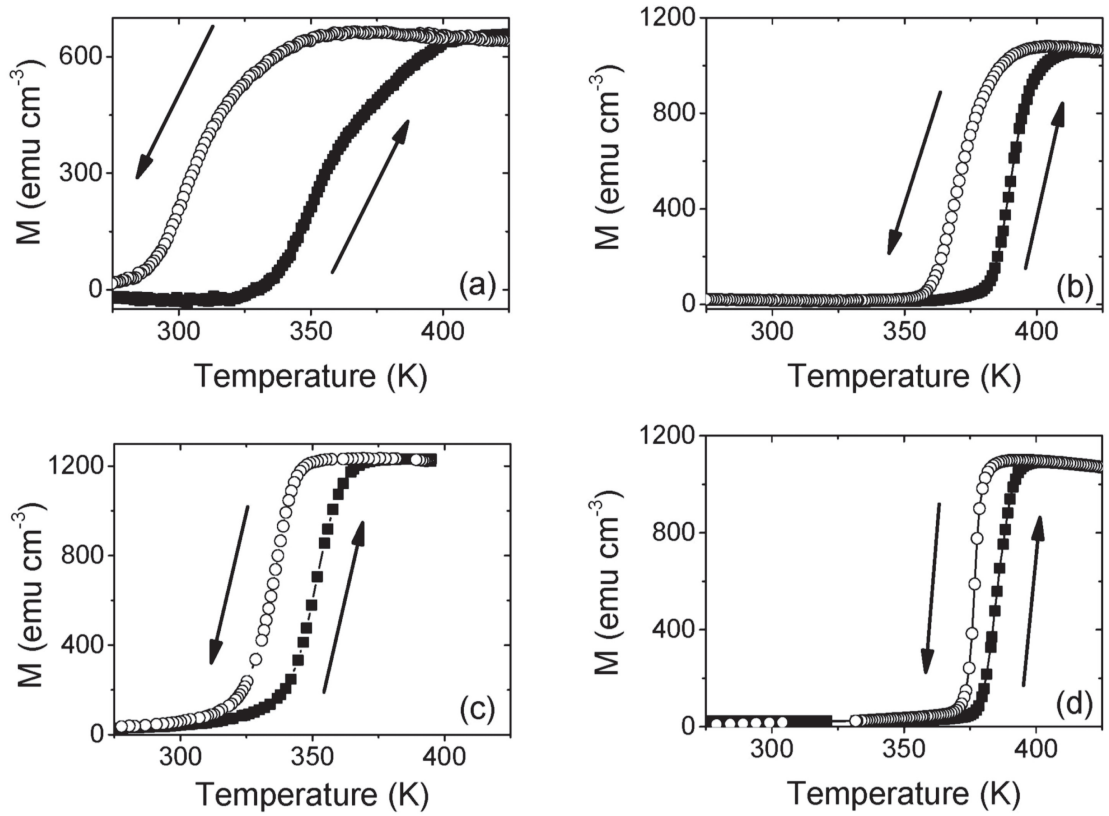

Figure 4. Temperature dependence of magnetic moment at an applied field of 1 T for the studied FeRh films with different thicknesses. (a) 6 nm, (b) 18 nm, (c) 36 nm, and (d) 100 nm.

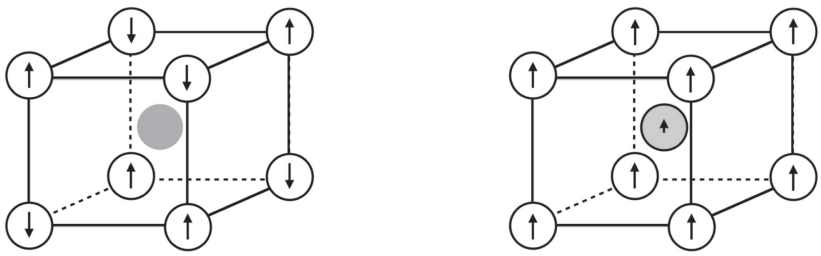

Figure 5. Structure of bulk FeRh. In the AF phase (left), the Rh atom (grey) has no magnetic moment while the Fe magnetic moments are ordered as indicated. Except for a different lattice constant (see text), the crystal structure remains unchanged in the FM phase (right); magnetic moment of the Rh atoms is then non-zero and parallel with that of Fe atoms.

The substrate (MgO) lattice constant is very well matched to FeRh. At room temperature, $a_{\mathrm{lc}}^{\mathrm{MgO}} = 0.4211$ nm [33] implies a mismatch of only $(a_{\mathrm{lc}}^{\mathrm{MgO}}/\sqrt{2} - a_{\mathrm{lc}}^{\mathrm{FeRh}})/a_{\mathrm{lc}}^{\mathrm{FeRh}} \approx -3 \times 10^{-3}$. Assuming that the in-plane lattice constants of FeRh (a_{xy}^{FeRh}) are dictated by the substrate and that the FeRh unit cell volume $(a_{xy}^{\mathrm{FeRh}})^2 a_z^{\mathrm{FeRh}}$ remains unchanged upon this deformation, we arrive at $a_{xy}^{\mathrm{FeRh}} = 0.2978$ nm and $a_z^{\mathrm{FeRh}} = 0.3002$ nm for the strained AF case and $a_{xy}^{\mathrm{FeRh}} = 0.2982$ nm and $a_z^{\mathrm{FeRh}} = 0.3030$ nm for the strained FM case.

The electronic structure of such bulk cubic or tetragonal FeRh crystal was calculated within the local density approximation with zero U and with spin–orbit interaction taken into account. Interband part of AC conductivity $\sigma_{\mathrm{inter}}(\omega)$ was then determined assuming Lorentzian broadening of 0.1 eV.

Interband and intraband terms

Permittivity spectra shown in figures 2(a) and (b) were calculated using WIEN2k taking into account only interband transitions through $\sigma_{\mathrm{inter}}(\omega)$. The complete expression for $\epsilon(\omega)$ reads

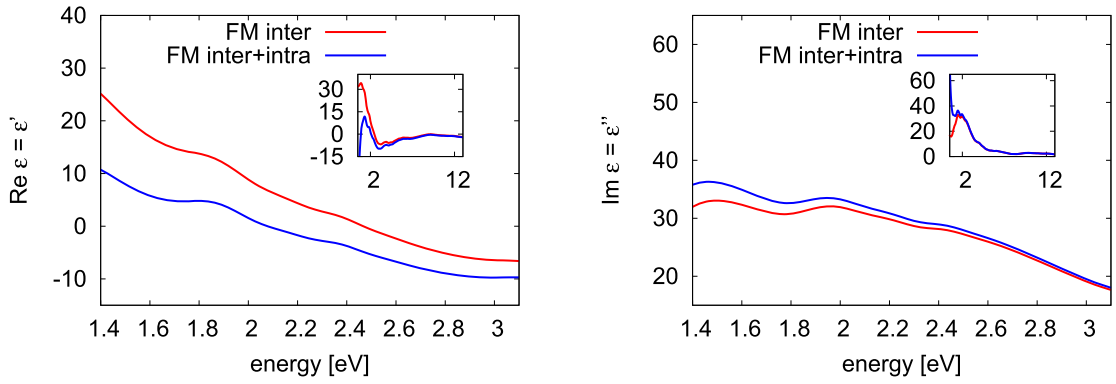

Figure 6. Permittivity $\epsilon\,(\omega) = \epsilon' + \mathrm{i}\epsilon''$ of bulk FeRh in the FM phase. Interband (last term in equation (1) only) and total (intraband plus interband) permittivity are shown. Insets show $\epsilon\,(\omega)$ in a broader spectral range.

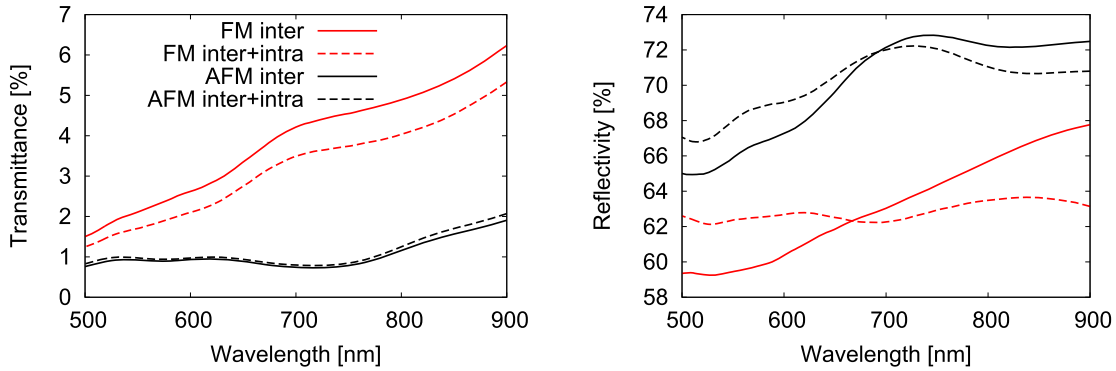

Figure 7. Transmittance and reflectivity for cubic FeRh calculated using permittivity shown in figure 6. Inclusion of the intraband contribution (dashed lines) does change the spectra quantitatively (data from figures 2(c) and (d) are replotted as solid lines) but the main conclusions remain unchanged: upon the transition from AF to FM, the transmittance (reflectivity) increases (decreases) and this change amounts to several per cent.

$$\epsilon\,(\omega)/\epsilon_0 = \epsilon_\mathrm{b} - \frac{\omega_\mathrm{p}^2}{\omega^2 + 1/\tau^2} + \frac{\mathrm{i}\omega_\mathrm{p}^2/\omega\tau}{\omega^2 + 1/\tau^2} + \frac{\mathrm{i}\sigma_\mathrm{inter}\,(\omega)}{\epsilon_0\omega}, \tag{1}$$

where ω_p is the plasma frequency and ϵ_b is the background relative permittivity stemming from high-energy transitions not accounted for in $\sigma_\mathrm{inter}\,(\omega)$. The plasma frequency given by equation (21) in [34] was determined to be $\hbar\omega_\mathrm{p} = 1.8$ and 5.5 eV for the AF and FM phase, respectively. The full $\epsilon\,(\omega)$ as in equation (1) calculated by WIEN2k has $\epsilon_\mathrm{b} = 1$.

Relaxation time can be estimated from the experimentally known DC conductivity on assumption that τ is the same for all bands contributing to the Drude formula $\sigma_0 = \omega_\mathrm{p}^2\epsilon\tau$. Taking $\sigma_0 = 110\ 00\ (\Omega\ \mathrm{cm})^{-1}$ for both FM and AF phases, total permittivity can be calculated using equation (1). Focusing on the experimentally investigated spectral range, $\epsilon\,(\omega) = \epsilon' + \mathrm{i}\epsilon''$ turns out to change only little in the AF phase when intraband transitions are included. In the FM phase, on the other hand, the differences are larger owing to the shorter relaxation times. Spectra of ϵ', ϵ'' shown in figure 6 indicate appreciable intraband corrections mainly to ϵ' at the largest wavelengths explored.

In spite of their significance on the level of $\epsilon\,(\omega)$, the inclusion of intraband terms does not change the reflection and transmission spectra qualitatively. The effect of adding intraband terms to T of the FM phase is to add an offset that grows steadily towards the long wavelengths as it is shown in figure 7(a). This effect is, nevertheless, smaller than the difference to the AF phase. Reflection spectra shown in figure 7(b) display a less clear trend yet it remains true that R decreases by a few percent upon the transition from AF to FM across the whole explored spectral range.

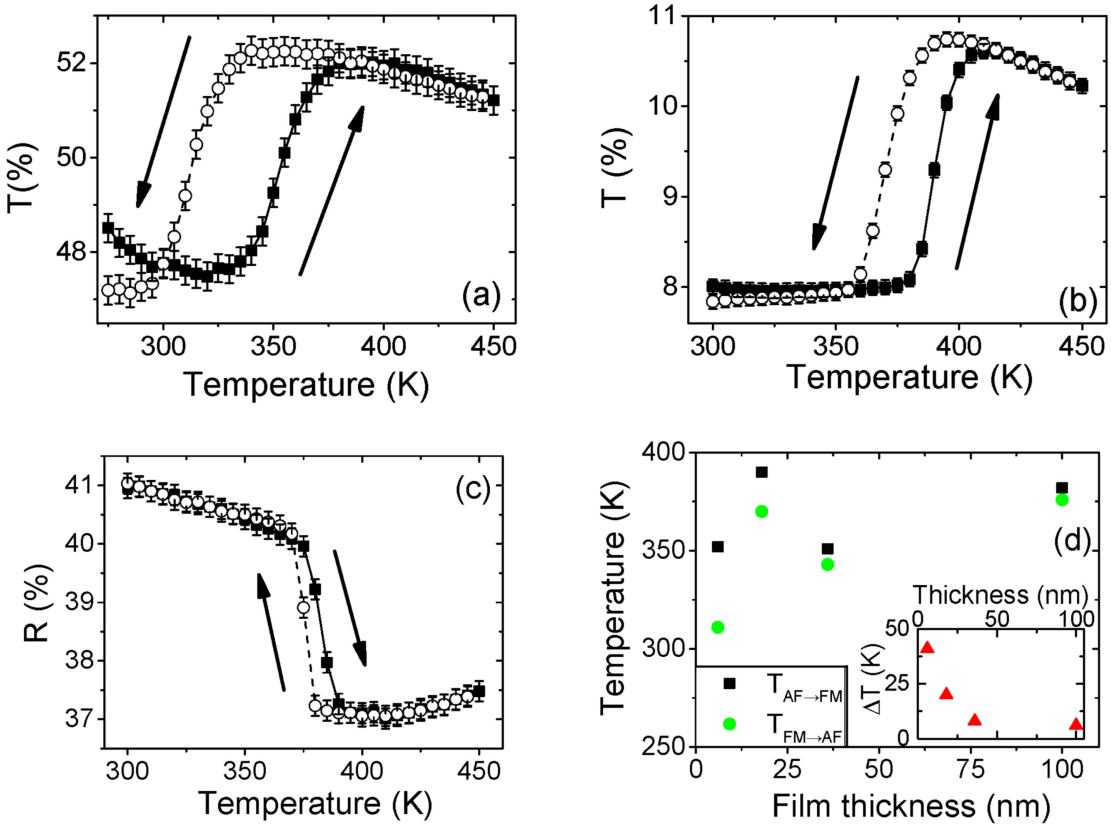

Figure 8. Change of optical properties of FeRh films with different thicknesses measured at 900 nm due to the temperature-induced phase transition. (a) Transmittance change for 6 nm film, (b) transmittance change for 18 nm film, and (c) reflectivity change for 100 nm film. (d) Dependence of the characteristic temperatures $T_{AF\rightarrow FM}$ and $T_{FM\rightarrow AF}$ on the film thickness. Inset: dependence of the hysteresis breadth $\Delta T = T_{AF\rightarrow FM} - T_{FM\rightarrow AF}$ on the film thickness.

Appendix C

In addition to figure 1 which concerns data for the 36 nm thick FeRh film, we show examples of the measured optical properties of other FeRh films in figure 8. As stated already in section 2, transmittance decreases with film thickness. Reflectivity increases from ≈35% for the 6 nm sample to ≈70% for the 18 and 36 nm samples. While all of this agrees with simple calculations of R and T based on the Fresnel formulae, reflectivity of the thickest sample shown in figure 8(c) was only about a half of what was expected. This is consistent with an observation that this sample had an unusually rough surface. Despite this, reflectivity and transmittance measured at a suitable wavelength can obviously be used, as figures 8(a)–(c) show, in lieu of magnetometry to monitor the AF-to-FM phase transition in all studied FeRh samples. To that end, we suggest that the kind reader compares the temperature-dependent data in panels (a)–(c) of figure 8 to that in panels (a), (b) and (d) of figure 4.

We show the inferred transition temperatures $T_{AF\rightarrow FM}$ and $T_{FM\rightarrow AF}$ in figure 8(d). Even though there is no fully systematic trend in the thickness dependence of the transition temperatures we observed that the hysteresis breadth $\Delta T = T_{AF\rightarrow FM} - T_{FM\rightarrow AF}$ shown in the inset of figure 8(d) decreases monotonously with the film thickness. The thickness dependence of the magnetic phase transition in FeRh was studied by several groups [4, 13, 14, 35]. Due to the complexities in the FeRh thin film preparation the obtained results are not always mutually compatible. However, one feature seems to be common to all the reported studies: the AF-to-FM transition seems to be less affected by the film thickness reduction than the FM-to-AF transition. In agreement with this we observed a considerably smaller reduction of $T_{AF\rightarrow FM}$ than that of $T_{FM\rightarrow AF}$ (by 65 K) when the film thickness was decreased from 100 to 6 nm (see figure 8(d)). The most plausible explanation of this phenomenon seems to be a different stability of the AF and FM phase in thin films—when the film thickness is reduced the FM phase is more stable [36].

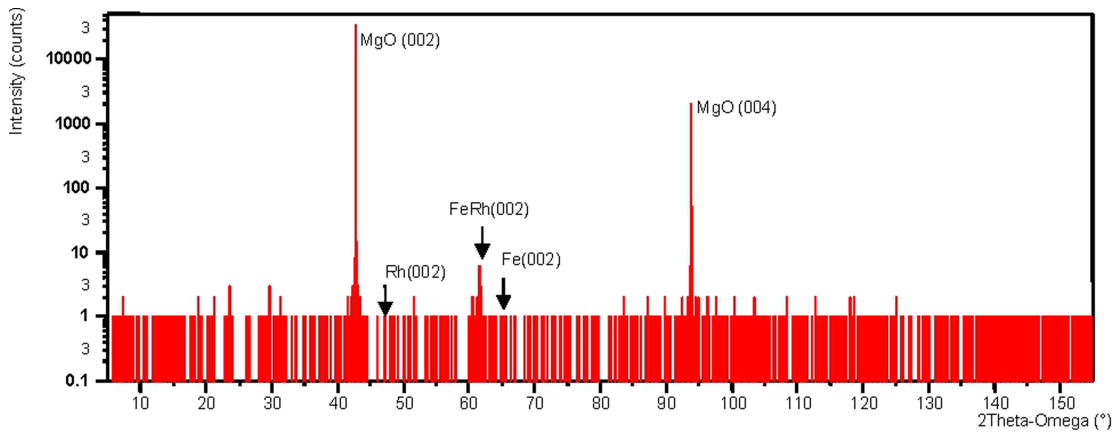

Figure 9. Symmetric $\theta/2\theta$-scan showing the presence of FeRh in the sample. There is no diffraction signal from a pure Rh/Fe phase.

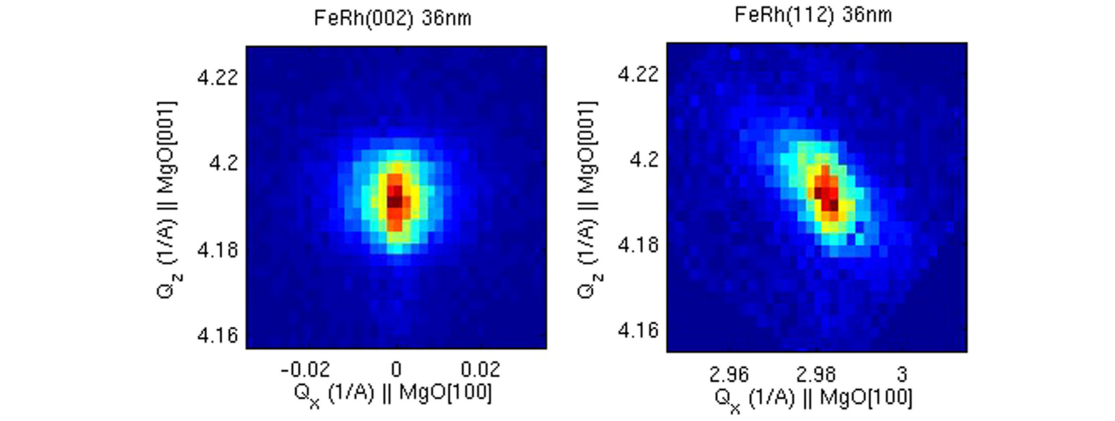

Figure 10. Reciprocal space map around FeRh(002) (left) and FeRh(112) (right).

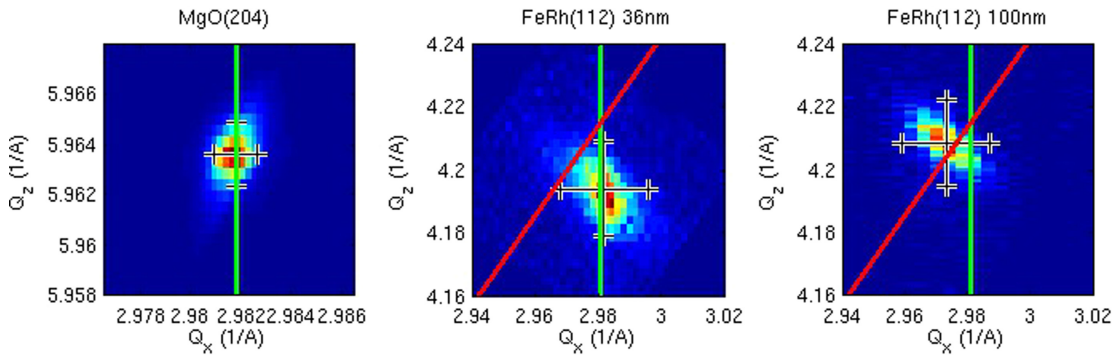

Figure 11. Reciprocal space maps of intensity distribution in the vicinity of MgO(204) (left subfigure) and FeRh(112) (middle and right figure) diffraction maxima. The Green line indicates the lateral coordinate of the substrate MgO(224) diffraction in a reciprocal space. Diffraction spot FeRh(112) in case of 36 nm thick sample lies on this green line (middle subfigure), i.e., the lattice is fully strained by the substrate. The red line indicates the reciprocal coordinates for the diffraction maxima of the (112) arbitrary cubic cell. Since the diffraction spot in case of 100 nm thick sample lies on this red line, the FeRh lattice in the thickest sample is fully relaxed.

Appendix D

All x-ray characterisations of FeRh thin layers on MgO substrates were performed using a standard coplanar high-resolution x-ray diffractometry. No external magnetic field was applied. In the incident path, there was an

elliptical x-ray mirror and a two-bounce Ge channel-cut monochromator. Since, the primary beam was monochromatised to Cu–K $_{\alpha 1}$ wavelength and parallelised in a diffraction plane having the angular divergence of 25 arc seconds. The diffracted beam was registered by a point detector behind a three-bounce Ge analyzer crystal making the angular acceptance to be 12 arc seconds in the diffraction plane.

Without an analyser crystal, we increased the angular acceptance of the detector to 1°. Since, it was possible to search for the crystallographic orientation of the FeRh with only an approximate Bragg angle of diffraction FeRh(002) and FeRh(112). The unit cell of annealed FeRh grown on MgO(001) substrate should orient in such a way that FeRh[001] (FeRh[110]) is parallel to MgO[001] (Mg[100]). Indeed, we found the (00L) diffraction maxima of FeRh layers and substrate in symmetrical $\theta/2\theta$-scan as shown in figure 9. Figure 10 shows the FeRh (112) and MgO(204) diffraction maxima that were found at expected coordinates for the reciprocal space at the equal sample azimuth.

In the high-resolution mode, we performed the reciprocal space mapping in the vicinity of the symmetric FeRh(002) and MgO(002) and asymmetric FeRh(112) and MgO(204) diffraction maxima. From the experimental data shown in figure 11, we concluded that FeRh layer is fully strained by the substrate, for all samples except the thickest one; the unit cell was tetragonally distorted with elongated *c*-axis perpendicular to the surface. The sample 100 nm thick exhibits a full relaxation of the FeRh lattice having a cubic symmetry.

References

[1] Fallot M and Hocart R 1939 *Rev. Sci.* **77** 498
[2] Krupička S, Maryško M, Jirák Z and Hejtmánek J 1999 *J. Magn. Magn. Mat.* **206** 45
[3] Thiele J-U, Maat S and Fullerton E E 2003 *Appl. Phys. Lett.* **82** 2859
[4] Thiele J-U, Maat S, Robertson J L and Fullerton E E 2004 *IEEE Trans. Magn.* **40** 2537
[5] Martí X *et al* 2014 *Nat. Mater.* **13** 367
[6] Shick A B, Khmelevskyi S, Mryasov O N, Wunderlich J and Jungwirth T 2010 *Phys. Rev.* B **81** 212409
[7] Cherifi R O *et al* 2014 *Nat. Mater.* **13** 345
[8] Lee Y *et al* 2015 *Nat. Commun.* **6** 5959
[9] Ju G, Hohlfeld J, Bergman B, van de Veerdonk R J M, Mryasov O N, Kim J Y, Wu X, Weller D and Koopmans B 2004 *Phys. Rev. Lett.* **93** 197403
[10] Kouvel J S and Hartelius C C 1962 *J. Appl. Phys.* **33** 1343
[11] Sasovskaya I I and Noskov M M 1974 *Fizika Tverdogo Tela (Solid State Phys.)* **16** 1853 (in Russian)
[12] Chen L Y and Lynch D W 1988 *Phys. Rev.* B **37** 10503
[13] Han G C, Qiu J J, Yap Q J, Luo P, Laughlin D E, Zhu J G, Kanbe T and Shige Y 2013 *J. Appl. Phys.* **113** 17C107
[14] Han G C, Qiu J J, Yap Q J, Luo P, Kanbe T, Shige Y, Laughlin D E and Zhu J G 2013 *J. Appl. Phys.* **113** 123909
[15] Yap Q J, Qiu J J, Luo P, Ying J F, Han G C, Laughlin D E, Zhu J G, Kanbe T and Shige Y 2014 *J. Appl. Phys.* **116** 043902
[16] Inoue S, Phuoc N N, Cao J, Nam N T, Ko H Y Y and Suzuki T 2008 *J. Appl. Phys.* **103** 07B312
[17] Rhee J Y and Lynch D W 1995 *Phys. Rev.* B **51** 1926
[18] Gray A X *et al* 2012 *Phys. Rev. Lett.* **108** 257208
[19] Cooke D W, Hellman F, Baldasseroni C, Bordel C, Moyerman S and Fullerton E E 2012 *Phys. Rev. Lett.* **109** 255901
[20] Sandratskii L M and Mavropoulos P 2011 *Phys. Rev.* B **83** 174408
[21] Palik E D 1998 Gallium Arsenide (GaAs) *Handbook of Optical Constants of Solids* vol 1 (Boston, MA: Academic) p 434
[22] Yeh P 1980 *Surf. Sci.* **96** 41
[23] Blaha P, Schwarz K, Madsen G K H, Kvasnicka D and Luitz J 2001 *WIEN2k, An Augmented Plane Wave + Local Orbitals Program for Calculating Crystal Properties* (Austria: Technische Universität Wien) (Karlheinz Schwarz)
[24] Nestell J E Jr and Christy R W 1980 *Phys. Rev.* B **21** 3173
[25] Roessler D M and Huffman D R 1998 Magnesium oxide (MgO) *Handbook of Optical Constants of Solids* ed E D Palik (Boston, MA: Academic) p 919
[26] Fan R *et al* 2010 *Phys. Rev.* B **82** 184418
[27] Maat S, Thiele J-U and Fullerton E E 2005 *Phys. Rev.* B **72** 214432
[28] Stamm C *et al* 2008 *Phys. Rev.* B **77** 184401
[29] Nuida T, Yamauchi T and Ohkoshi S 2011 *J. Appl. Phys.* **110** 063516
[30] Rameev B *et al* 2006 *Phys. Status Solidi* a **203** 1503
[31] Khan M A 1979 *J. Phys. F: Met. Phys.* **9** 457
[32] Ibarra M R and Algarabel P A 1994 *Phys. Rev.* B **50** 4196
[33] Smith D K and Leider H R 1968 *J. Appl. Cryst.* **1** 246
[34] Ambrosch-Draxl C and Sofo J O 2006 *Comput. Phys. Commun.* **175** 1
[35] Suzuki I, Koike T, Itoh M, Taniyama T and Sato T 2009 *J. Appl. Phys.* **105** 07E501
[36] Lounis S, Benakki M and Demangeat C 2003 *Phys. Rev.* B **67** 094432